POTENTIAL SEMICONDUCTOR MATERIALS FROM IRRADIATION OF SILICON DIOXIDE (SiO_2): EFFECT OF X-RAY EXPOSURE ON THE STRUCTURE THROUGH ACID PRECIPITATION METHOD

Dhita ARIYANTI[1*], Renaldy Bernardo SARAGIH[1], Sherina Massayu PUTRI[1], Nikita SALSHABILA[1], ISMAIL[2], Ayu Jati PUSPITASARI[2], Abdul WAFI[3], Sidik PERMANA[4]

This paper aims to determine the effect of X-ray radiation on the structure of silica dioxide (SiO_2) obtained from sodium silicate (Na_2SiO_3) through the acid precipitation method. The variations of cyan-X energy used are 0 KeV, 120 KeV, 170 KeV, and 220 KeV. Characterization was carried out using X-ray diffraction (XRD) to analyse changes in crystal structure, Fourier Transform Infrared Spectroscopy (FTIR) to identify changes in chemical bonds, and Particle Size Analyzer (PSA) to evaluate particle size distribution. XRD results showed before X-Ray irradiation, it showed that combined phase of crystallin (tridymite and cristobalite) and amorphous of SiO_2. While, after irradiation processing, intensity of amorphous SiO2 is increased and the crystalline phase is decrease drastically. It may cause that energy of X-Ray had broken the Si–O bonds in the surface area and reform the crystalline form to amorphous phase, FTIR analysis revealed modifications in the Si–O–Si group, and PSA results showed that the higher the X-ray voltage, the greater the particle size due to dislocation and defects. From the results of this study, it can be concluded that SiO_2 can be produced from Na_2SiO_3, and X-ray radiation can convert the structure of SiO_2 into amorphous, which has the potential to increase its efficiency as a semiconductor material. However, further research is needed to evaluate the thermal conductivity, charge capacity, and stability of materials in order to optimize applications in electronic technology.

Keywords: silicate dioxide, sodium silicate, x-ray, semiconductor

[1]* Department of Nuclear Chemical Engineering, Polytechnic Institute of Nuclear Technology, National Research and Innovation Agency, Babarsari Street PO BOX 6101 YKBB Yogyakarta 55281, Indonesia, (corresponding author: dhit001@brin.go.id)
[2] Research Center for Safety, Metrology, and Nuclear Quality Technology, National Research and Innovation Agency, Serpong, Indonesia
[3] Research Center for Food Technology and Processing, National Research and Innovation Agency (BRIN), Gading, Playen, Gunungkidul, Yogyakarta 55861, Indonesia
[4] Nuclear Engineering, Faculty of Mathematics and Natural Sciences, Bandung Institute of Technology, Ganesha 10 Street, Bandung, 40132, Indonesia

1. Introduction

1.1. Semiconductor Material and Future Prospect

Semiconductor materials are substances that have electrical conductivity between that of conductors and insulators. They form the foundation of modern electronics and are crucial for various applications in power electronics, wearable devices, photocatalysis, and transistors [1-4]. The demand for semiconductor materials has intensified due to the rapid development of artificial intelligence, microchips, and other advanced technologies [5].

Although semiconductors are essential for technological progress, their production is not environmentally friendly. This has led to a growing emphasis on sustainable practices in semiconductor fabrication, including recycling and reducing emissions [5]. Additionally, the semiconductor industry faces challenges related to water scarcity, prompting the development of water reclamation technologies to meet the high water demands of manufacturing processes [4]. Semiconductor materials are urgently needed across various sectors, from consumer electronics to industrial applications.

The future prospects of semiconductors include the development of wide bandgap materials for improved power electronics [1], the use of 2D materials in wearable energy sources [6], and the creation of heterostructures for enhanced photocatalytic efficiency [3]. Furthermore, there is a growing focus on sustainable practices and innovative packaging solutions to address environmental concerns and meet the increasing demand for high-performance semiconductor devices [5,7].

1.2. Silicon Dioxide as Semiconductor Material

Silicon dioxide (SiO_2) can be used as a semiconductor material, particularly in its amorphous form, and can be extracted from sodium silicate through various processes. SiO_2 is widely used in semiconductor applications due to its excellent insulating properties and ability to form high-quality interfaces with silicon. In the semiconductor industry, SiO_2 is commonly used as a gate dielectric in metal-oxide-semiconductor field-effect transistors (MOSFETs) and as an insulating layer in integrated circuits [8]. The amorphous nature of SiO_2 allows for uniform electrical properties and reduces defects in the material, making it suitable for various electronic applications.

SiO_2 can be extracted from sodium silicate (Na_2SiO_3) through different methods, each with its own advantages. One method involves precipitation silica nanoparticles using supercritical CO_2, where CO_2 acts as both an antisolvent and a reactant [9]. Another approach uses a simple solution method to synthesize amorphous silica from sodium silicate, which can then be dispersed in various agents for applications such as paint coatings [10]. The extraction of SiO_2 from

sodium silicate and its subsequent use as a semiconductor material demonstrates the versatility of this compound. The precipitation method can be used [9], and the solution method for synthesizing [10] are two effective approaches for obtaining SiO_2 from sodium silicate. These methods allow for the production of high-quality SiO_2 suitable for semiconductor applications, highlighting the importance of sodium silicate as a precursor in the semiconductor industry.

Sodium silicate can be from municipal solid waste incineration bottom ash [11]. Similarly, rice husk ash from agricultural waste has been employed to synthesize sodium silicate [12]. Coal gasification coarse slag, typically destined for landfills, can be transformed into high-modulus, low-impurity sodium silicate using a novel acid activation depolymerization–dilute alkali dissociation method [13]. Sodium silicate derived from waste materials shows promise in various applications; this study uses it as the main component of making silicon dioxide (SiO_2). This highlights the importance of carefully considering the specific application and environmental conditions when utilizing waste-derived sodium silicate.

1.3. Best Semiconductor Characteristic

High-mobility semiconductors are sought to replace silicon in the microelectronics industry as silicon-based transistors approach their physical limits. Both bulk materials (like silicon-germanium and III-V semiconductors) and low-dimensional nanomaterials (such as carbon nanotubes and transition metal dichalcogenides) have been explored [7]. The key characteristics of a good semiconductor material include high mobility, low effective mass, and a high-quality native oxide as a dielectric counterpart with strength and a high-quality band gap.

Semiconductor materials possess several key characteristics that make them suitable for various electronic applications:

- **Bandgap**: The most crucial property of a semiconductor is its bandgap, which determines its electrical and optical properties. Wide-bandgap semiconductors like SiC, GaN, and diamond offer superior performance for high-power applications due to their ability to handle higher blocking voltages, switching frequencies, and efficiency [14]. The bandgap can be tuned through various methods, such as controlling layer numbers, heterostructuring, strain engineering, and chemical doping, especially in 2D materials [15].

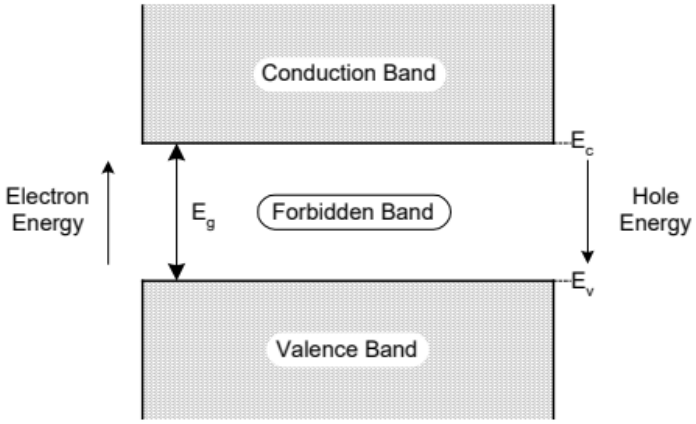

Fig. 1. Simplified energy band diagram of a semiconductor (A. Chaves *et al*., 2020) [15].

- **Crystal Shape**: For practical applications, the ability to dope a material is governed by intrinsic properties such as absolute band edge positions and defect formation energies [16]. Amorphous materials have emerged as promising candidates for improving semiconductor performance due to their unique structural and electronic properties. Amorphous oxide semiconductors, in particular, have gained attention for their potential in display panels and monolithic 3D applications [17]. The disordered structure and thermodynamic metastability of amorphous inorganic semiconductors contribute to their distinctive electrical and optical properties, making them suitable for various technologies including solar cells, photoelectrocatalysis, and photocatalysis with high strength and good irradiation tolerance [18].

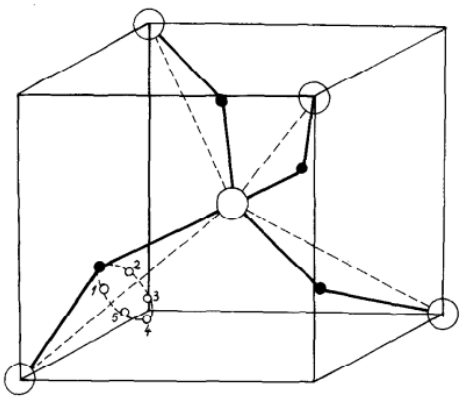

Fig. 2. Local atomic shape arrangement in SiO_2 crystalline (E. Görlich, 1982) [19].

- **Chemical Bond**: The Si-O and Si-O-Si bonds play crucial roles in determining the properties and characteristics of SiO_2 materials, which in

turn affect semiconductor performance. The structure of SiO_2 is primarily composed of SiO4 tetrahedra units, with Si-O bonds forming the backbone and Si-O-Si bonds connecting these units [20]. The Si-O bond length is typically around 1.62 Å, while the Si-O-Si bond angle is estimated to be 147±10° [21]. This structural characteristic can affect the material's behavior in semiconductor applications. The Si-O and Si-O-Si bonds also play a role in defect formation and charge trapping, which are critical for semiconductor performance. For instance, a SiO_2 tetrahedra unit with a wide O-Si-O angle (≥132.0°) can act as an electron trapping site in unstrained amorphous SiO_2 [22]. Additionally, under uniaxial tensile strain, a SiO4 unit with a wide O-Si-O angle and a long Si-O bond (≥1.660Å) can form a novel intrinsic electron trap [22]. These defects can significantly impact the electrical performance of semiconductor devices.

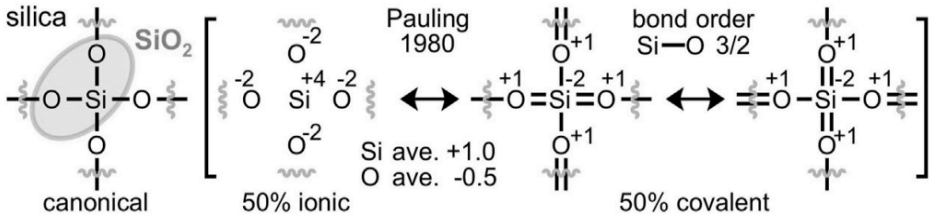

Fig. 3. Pauling's resonance hybrid model of α-quartz silica, SiO_2 (S. A. Miller, 2023) [20].

- **Structural properties**: The structural characteristics of semiconductors play a crucial role in their performance. For instance, bismuth-bearing III-V semiconductor alloys have been investigated for their potential as narrow-gap materials with improved structural properties compared to current infrared detection materials [23]. On the size particle aspect, smaller particle sizes generally offer advantages for semiconductor materials. In the case of colloidal semiconductor nanocrystals, smaller particle sizes lead to stronger quantum confinement effects, which can be beneficial for tuning optical and electronic properties. Ferreira et al. [24] discuss how the bandgap of semiconductor nanocrystals is size-dependent, with smaller particles typically exhibiting larger bandgaps due to quantum confinement. This allows for precise control of optical properties by adjusting particle size [24]. For lithium-ion battery electrodes, Bläubaum et al. [25] report that narrower particle size distributions with smaller particles generally result in better cell performance, including improved charge/discharge characteristics, capacity, efficiency, and cycling stability. However, this trend has a lower limit, as extremely small particles can negatively affect performance [25]; smaller particles (62-306 nm range) yielded much better adjuvant effects than larger particles. This

demonstrates that the benefits of smaller particle sizes can extend beyond traditional semiconductor applications [26].

- **Magnetic properties**: Some semiconductors, such as Mn-based III-V and II-VI diluted magnetic semiconductors, exhibit carrier-controlled ferromagnetism, which is valuable for spintronics applications. Mn-based III-V and II-VI are materials that exhibit carrier-controlled ferromagnetism. III-V semiconductors are composed of elements from group III (such as gallium or indium) and group V (such as arsenic or phosphorus) of the periodic table, while II-VI semiconductors consist of elements from group II (such as zinc or cadmium) and group VI (such as sulfur or selenium) [27].

Other materials, such as p-type oxide semiconductors [28] and strained Ge channels on SiO_2 virtual substrates [29], are being explored to enhance semiconductor device performance and expand their applications in various fields. In the test, all of the above indicators can be produced with an important instrument, namely X-ray diffraction (XRD), to determine the crystal structure, besides that to determine the particle content and chemical bonds and the condensation they contain, Fourier Transform Infrared Spectroscopy (FTIR), then finally the Particle Size Analyzer (PSA) can also be used to find out the amount of particles contained, the results of the three tests can support each other and be associated with each other to Conclusions of the study.

1.4. Irradiation Used for Improvement Properties Materials

Several studies have evidenced that electromagnetics wave improved material's performance [41-43]. X-ray radiation has been utilized to improve the properties of silica dioxide materials and develop semiconductor materials. However, X-ray exposure and semiconductor performance are complex and depend on various factors [30].

In previous research, oxide thin film transistors (TFTs) based on gallium indium zinc oxide have demonstrated superior X-ray radiation hardness compared to organic TFTs. When exposed to X-ray radiation, flexible oxide TFTs maintained a constant mobility of 10 $cm^2\ V^{-1}\ s^{-1}$ even after exposure to doses of 410 krad, while organic TFTs lost 55% of their transport performance [31]. This exceptional resistance to ionization damage is attributed to the intrinsic properties of oxide semiconductors.

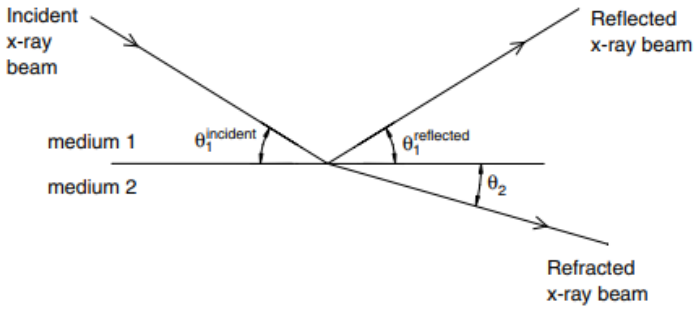

Fig. 4. Sketch of the theoretical conditions for X-ray (L. A. September, 2023) [32]

This semiconductor has good-strength materials, tunable band gaps, and amorphous effective crystal growth via solution processes [33]. However, it's important to note that while these materials are excellent for X-ray detection, the impact of X-ray radiation on their long-term performance and stability needs further investigation. In conclusion, while X-ray radiation can be used to study and potentially improve certain semiconductor materials, particularly in terms of radiation hardness, it is not a universal method for enhancing semiconductor performance. The effects of X-ray radiation on semiconductors are highly dependent on the specific material and its intended application.

2. Materials and Methods

2.1. Preparing materials and tools

This study utilizes sodium silicate (Na_2SiO_3) with a purity level of 99.90% as a base material, hydrochloric acid (HCl) and water. The tools used in this study include glass instrumentation, namely beaker cups, measuring flasks, magnetic stirrers, separation funnels, thermometers, stirring rods, analytical scales, ovens, and the use of ionizing radiation on samples is carried out using an X-ray aircraft with a voltage range of 0 KeV to 250 KeV. After solution preparation, the next step is characterization using some instruments such as X-Ray Diffraction (XRD), Particle Sizer Analysis (PSA), and Fourier Transform Infrared (FTIR).

2.2. Conversion of sodium silica (Na_2SiO_3) to silica dioxide (SiO_2) by acid precipitation method with HCl

The first step was weighed 12 mg sodium silicate (Na_2SiO_3) using an analytical balance and transferred into a glass beaker. It was then dissolved in 150 ml of distilled water to obtain a homogeneous solution. Separately, 50 ml of 2 M hydrochloric acid (HCl) solution was prepared by diluting 36% w/w concentrated HCl stock solution with distilled water. This 2 M HCl solution was used for the precipitation process.

The HCl solution was added dropwise to the Na_2SiO_3 solution while continuously stirring with a magnetic stirrer to prevent localized precipitation and ensure uniform mixing. The addition continued until the pH of the solution decreased to approximately 6.5, which was monitored using a calibrated digital pH meter. Minor adjustments were made by adding either additional HCl or distilled water to precisely reach the target of pH.

Once the desired pH was achieved, the resulting silica (SiO_2) precipitate was filtered from the liquid phase. The precipitate was subsequently washed three times with distilled water to remove residual ions and impurities. After washed, the SiO_2 precipitate was dried in an oven at 65°C for 1 hour. This drying step was sufficient to remove moisture content without inducing structural changes or thermal degradation of the SiO_2.

2.3. Material Modification

SiO_2 is put into plastic clips with each weight of 8 grams. This initial stage is important to ensure that the material is in a ready-to-use condition before proceeding with the experimental process. Then, SiO_2 is fired ionizing radiation using an X-ray aircraft with several voltage variations, namely 120 KeV, 170 KeV, and 220 KeV in the same time range, namely 15 minutes at a distance of one meter from the source of the X-ray aircraft.

2.4. Characterization

After the SiO_2 has been fired X-ray radiation according to the specified exposure energy, then the characterization process is carried out on the SiO_2 that has been fired to observe the changes or results that occured. Characterization of SiO_2 semiconductor materials is carried out using FTIR, PSA, and XRD. The use of FTIR aims to identify changes in functional groups in SiO_2 after exposure to X-rays. Furthermore, an analysis was carried out using PSA to evaluate the size distribution of SiO_2 particles both before and after X-rays. Finally, the characterization uses XRD to analyze the crystal structure of the formed SiO_2. The IR spectra were recorded using a “Bruker Alpha" Fourier Transform Infrared (FTIR) spectrophotometer, operating in the range of 4000–400 cm^{-1}. The Attenuated Total Reflectance (ATR) technique was employed to measure the surface functional groups of the SiO_2 powders without any special sample preparation.

Particle size distribution was analyzed using a “Malvern Mastersizer 3000" Particle Size Analyzer (PSA), employing laser diffraction with a green visible light source ($\lambda \approx 532$ nm). Measurements were based on D90 values, representing the diameter below which 90% of the sample volume exists. The samples were dispersed in deionized water prior to measurement to avoid agglomeration and to ensure accurate sizing. The crystalline structure of the

samples was characterized using an X-Ray Diffraction (XRD) system, specifically a “Rigaku" diffractometer equipped with a Cu Kα radiation source (λ = 1.5406 Å), operating at 40 kV and 30 mA. Data were collected over a 2θ range of 10° to 80° with a step size of 0.02° and a scanning speed of 2°/min. XRD analysis was used to determine the phase composition and degree of crystallinity of the SiO_2 samples before and after irradiation.

After characterization, an evaluation is carried out regarding the need for modification. If modifications are evident in the initial method or procedure used, the data resulting from the direct characterization is collected and stored for further analysis process. The data is then interpreted to obtain relevant conclusions according to the research objectives.

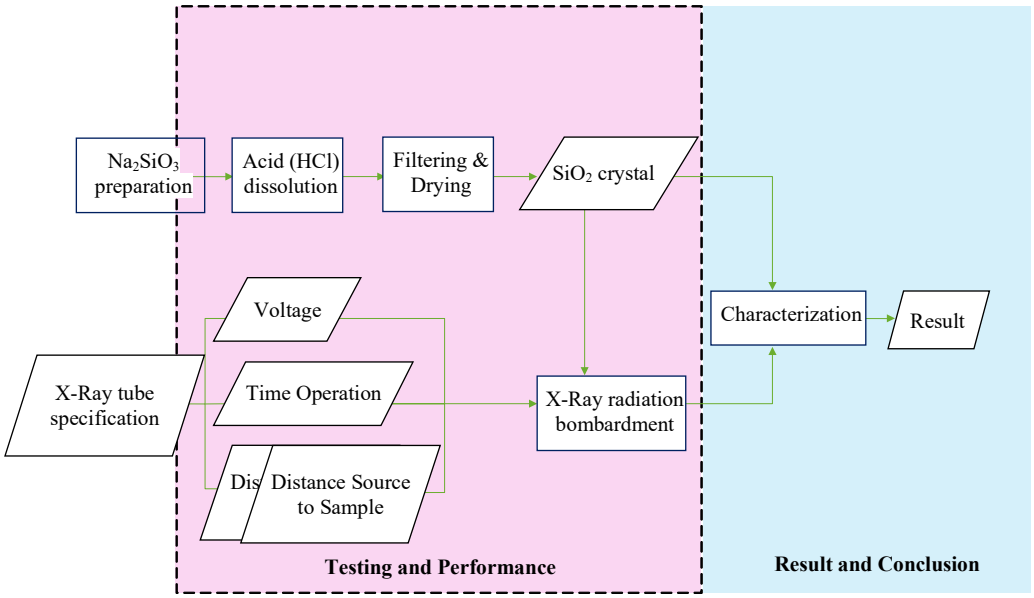

Fig. 5. Work flowchart

3. Results and discussion

3.1. X-Ray Diffraction Result

A crystal is characterized by a regular succession of basic units: atoms, ions or molecules, in a periodic three-dimensional network [44]. Crystalline and amorphous materials differ significantly in their atomic structure and resulting properties. Crystalline materials possess long-range periodic order in their atomic arrangement. For amorphous material the atomic arrangement is more like liquid and has no long-range periodicity [34,35].

The differences between crystalline and amorphous materials significantly impact their properties. Crystalline metals generally exhibit good deformability

but low strength and poor irradiation tolerance, while amorphous materials often display poor deformability but high strength and good irradiation tolerance [36]. These distinctions in structure and properties make the study of crystalline-amorphous hybrid structures particularly interesting, as they can potentially combine the advantages of both ordered and disordered components, leading to emergent collective properties [37].

XRD works by observing the diffraction pattern produced when a monochromatic beam of X-rays is scattered at specific angles from each set of lattice planes in a sample[38] [39]. The 2θ (two-theta) function in XRD refers to the angle between the incident X-ray beam and the diffracted beam. This angle is crucial in determining the interplanar spacing of the crystal lattice, as described by Bragg's law [40]. The diffraction pattern, including the positions (2θ angles) and intensities of the diffraction peaks, correlates to a specific crystal structure [40].

In the results of research that has been carried out using XRD, 4 types of sample tests are carried out based on variations in X-ray ionizing radiation energy. In samples with an energy of 0 keV or without exposure to X-ray radiation, a diffractogram with a peak was obtained to illustrate that SiO_2 at 0 keV energy is mixed in amorphous and crystalline phase. It matches with ICSD 98-016-2660 where there is a gentle slope at $2\theta = 22.5873^{\circ}$ which indicates that the SiO_2 formed is an amorphous phase [45]. Moreover, several kinds of structures can be present in both crystalline and amorphous phases. The structure factor (SF) obtained from the experimental scattering intensity depends directly on the fraction of crystallites and their sizes. As they grow, the half-width of peaks decreases. The height of peaks of the corresponding crystalline phases increases with their volume fraction. At the same time, the SF of the amorphous phase becomes less clearly pronounced [46].

From the result of diffractograms 0 keV, it showed that combined phase of crystallin (tridymite and cristobalite) and amorphous of SiO_2. This statement was supported by intensity before and after exposure of X-Ray irradiation. Intensity of amorphous SiO_2 before exposure less than 3000 counts. While, after irradiation processing, intensity of amorphous SiO_2 is 3000 counts. It may cause that energy had broken the Si–O bonds in the surface area and reform the crystalline form to amorphous phase.

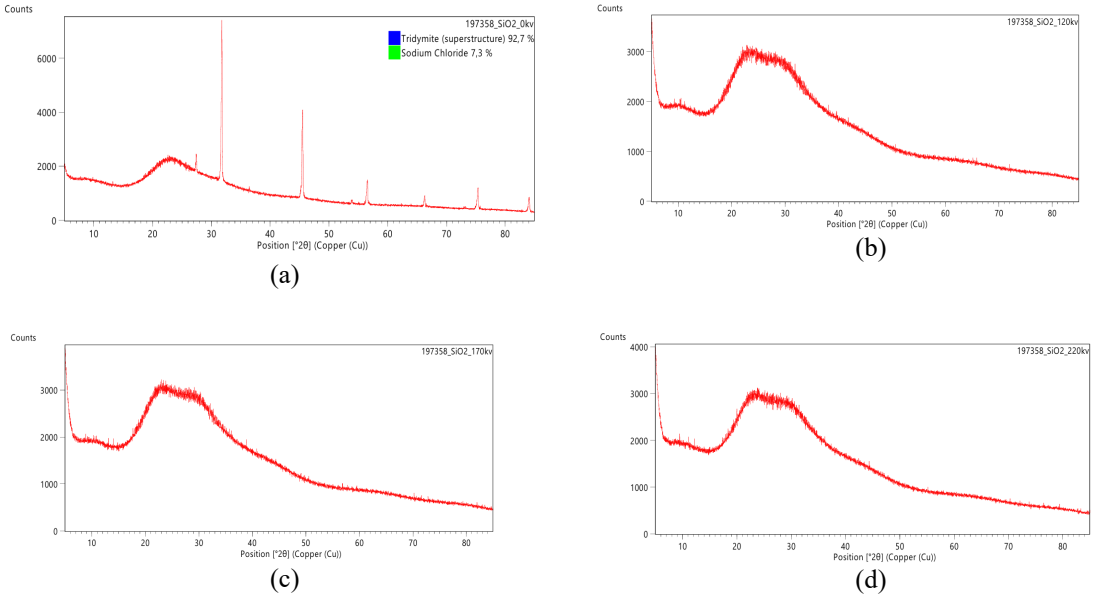

Fig. 6. Diffractograms, a) 0 keV; b) 120 keV; c) 170 keV; d) 220 keV

Then, in samples with ionizing radiation energies of 120 keV, 170 keV, and 220 keV, a diffractogram showed that the sample was not crystalline (amorphous). The XRD diffractogram of irradiated SiO_2 samples at energies of 120 keV, 170 keV, and 220 keV, as shown in **Figure 6**, does not have the specific and pointed peaks of samples with energies of 0 keV. The interaction of X-ray with SiO_2 produces a photoelectric effect by not ruling out the possibility of a Compton effect. The photoelectric effect will cause SiO_2 to experience an increase in the number of electrons, and the addition of electrons will affect the structure of SiO_2. Crystal structures that have become amorphous may produce content with different chemical bonds than SiO_2 samples described in **Section 3.2.**

Among the various types of changes in crystal structure due to the influence of X-ray ionizing radiation will cause *defects* in the SiO_2 crystal, as the amount of X-ray energy intensity given will be proportional to the exponent of the thickness or morphology of the crystal itself. The three energy ranges used are enough to *bombard the* SiO_2 crystal so that a defect appears in the crystal, changing the lattice angle from the total eight tetragonal lattice angles to the loss resulting from the 2θ diffractogram.

$$I = I_0 e^{-\mu x} \tag{1}$$

The amorphous properties found in SiO_2 crystals will result in higher thermal conductivity values compared to their crystalline structure. In addition,

the strength of the material with amorphous properties will increase, and the distance between the valence band and the conduction band in the *gap band* will be closer. These three results are needed to produce better-quality semiconductor materials.

3.2. Fourier Transform Infrared (FTIR) Result

Silica dioxide (SiO_2) in this study has a peak spectrum at typical wavelengths of 1057 cm^{-1} and 1110 cm^{-1} with symmetrical wave characteristics due to molecular vibrations with large Gaussian numbers. After the shooting using X-rays, the appearance of peaks at a certain wavelength change.

Based on **Figure 7** and **Table 1**, in silica dioxide samples exposed to X-rays at a voltage of 120 keV, the spectrum is disturbed so that small peaks (resembling falls) in the spectrum range of 500–750 cm^{-1}. The large band around 3400 cm^{-1} is due to the presence of the water. It might be possible that the samples were not dried sufficiently, both the time and the temperature used. So, the SiO_2 unvaporized perfectly.

In SiO_2 samples that are exposed to X-rays at voltages of 170 keV and 220 keV have similar spectrums. Similar measurement figures can be seen in the Si–O–Si bond range and in the N–H bond range. This is due to the crystal effect that undergoes a transition of shape to amorphous (*defect*); therefore, the molecule will undergo *vibration*, which is irregular and moves freely at the degree of increase in density, resulting in spectral melting. A new weak peak observed around 2314 cm^{-1} in the FTIR spectra of irradiated SiO_2 samples may indicate the formation of carbon related species, such as C≡C triple bonds or C=C double bond. High-energy X-ray irradiation can induce bond breakage and defect formation, potentially facilitating the incorporation of carbon fragments surface. Although atmospheric CO_2 typically contributes signals in this region, the consistent appearance of this peak following irradiation suggests that structural modifications associated with irradiation cannot be entirely ruled out. Further chemical analysis is required to definitively confirm the presence of carbon radicals. This is due to the vibration (*vibration*) of the material, which experiences increased sensitivity as the applied voltage increase*s.* This effect appears at voltages starting at 170 keV or in the range above 120 keV, so further research is needed using voltages between the range of 120 keV to 170 keV to find out at what voltage carbon radicals begin to appear and at what energy this effect ends.

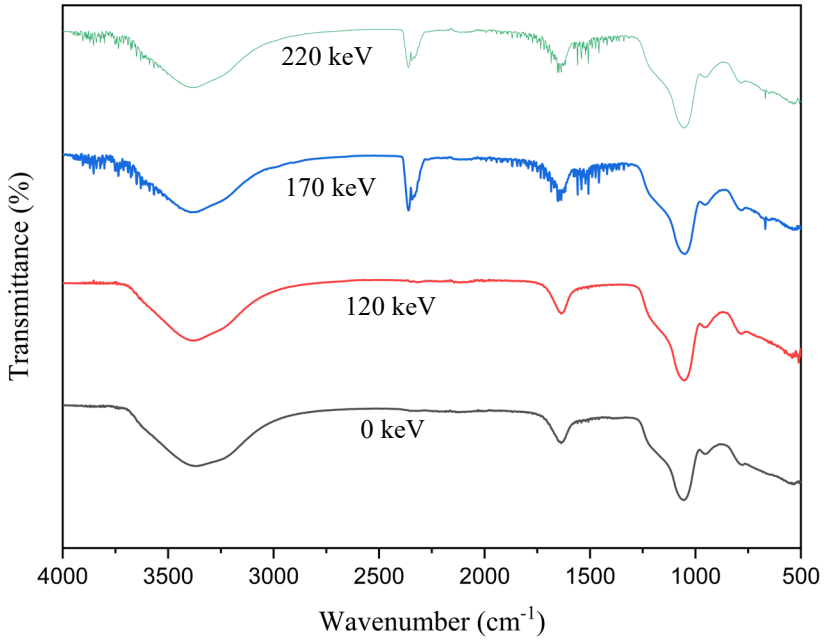

Fig. 7. Spectral results at separate dose variations

Table 1.

FTIR Results with Physical Characteristic

No	Wavelength (cm^{-1})	Bonding	Function Cluster Name	Information
1.	1110	Si – O	Silica oxide	Symmetric
2.	1057	Si – O – Si	Silica dioxide	Symmetric
3.	1653	C = O	Carbon dioxide	Symmetric
4.	2314	C≡C / C=C	Carbon triple bond/double bond (carbon related species)	Asymmetric
5.	3348	O–H	Trapped water that vaporized perfectly during drying processing	Symmetric

X-ray exposure also affects the chemical bonds in SiO_2 materials. The increased energy in the range of 120 KeV to 220 KeV is not spared from the occurrence of a Compton effect that can break Si–O and can be replaced by a new unstable bond, for example, the C-C bond at a wavelength of 2314 cm^{-1}. These radicals can affect the density of the material, in addition to the presence of significant peak drops at high X-ray aircraft voltages, which also indicate that the density level is getting bigger and causes the crystal to be very sensitive to vibration (*vibration*). The increase in material density and the modification of crystals into amorphous from the point of view of FTIR testing is very promising for the use of this modified SiO_2 as a technologically advanced material in the semiconductor field.

3.3. Particle Sizer Analysis (PSA) Result

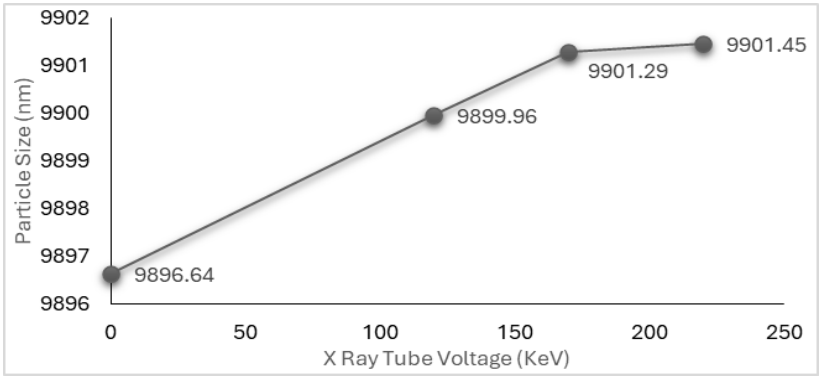

Fig. 8. Particle size analyser result

The particle size analyzer (PSA) is used to investigate the extent to which X-ray radiation affects the morphological state related to the size of the SiO_2 crystal lattice. PSA measures SiO_2 particles using visible light on the green spectrum, with a total reading of 90 times (D90), which is interpreted as an average of 90 data spreads. This amount of data is intended to increase the level of accuracy through the distribution of data from instrument readings.

From the available data, the higher the tension of the X-ray tube given to the sample, the higher the particle size data, which means that in this study, the tension is directly proportional to the particle size. The data on the sample with a voltage value of 0 KeV (without X-rays being fired) shows data of 9896.64 nm and an increase in particle size of 3.32 nm to the sample given X-ray radiation at a voltage of 120 KeV, the difference in particle size decreases at a voltage of 170 KeV to 120 KeV, which is 1.33 nm, then the value decreases at a voltage of 170 KeV which causes the graph to appear sloping, This is in accordance with the exponential principle of X to I so that it can be concluded that the higher the voltage of the X-ray plane to radiate the SiO_2 sample, the larger the crystal particles will be, this is suspected to be due to the occurrence of dislocations and *defects*, as evidenced by the results of XRD and FTIR.

Actually, the amount of particles needed to become a good semiconductor material is smaller particles because they have a high level of efficiency and charge, but in terms of quality *of the band gap,* the larger particle size is considered to be more profitable, in terms of the physical and chemical properties above, it is necessary to carry out further specific tests to determine the level of efficiency which includes, thermal conductivity, charge capacity, material stability, as well as *band gap.*

4. Conclusion

This study presents the results of characterization using an X-ray diffractometer, Fourier transform infrared, and particle sizer analysis to determine the success of SiO_2 synthesis from Na_2SiO_3 and the effect of X-ray radiation on the structure of SiO_2. Na_2SiO_3 has been successfully fully converted to SiO_2. Then, from the results of the XRD, it can also be known that X-ray radiation can affect the structure of the crystals and turn them into an amorphous form. Our findings prove that SiO_2 can be obtained from Na_2SiO_3, which can increase the compound's functional value. X-ray radiation can also change the structure of crystalline SiO_2 to amorphous SiO_2,

Before X-Ray irradiation, it showed that the combined phase of crystallin (tridymite and cristobalite) and amorphous of SiO_2. While, after irradiation processing, the intensity of amorphous SiO_2 is increased and the crystalline phase is decrease drastically. It may cause that energy of X-Ray had broken the Si–O bonds in the surface area and reform the crystalline form to amorphous phase. This phenomenon is more advantageous in semiconductor applications. However, further research is needed to determine and evaluate the material's thermal conductivity, charge capacity, and stability.

Acknowledgements

We expressed deepest gratitude to the Polytechnic Institute of Nuclear Technology and the Indonesia Research and Innovation National Agency for supporting and providing research equipment until the testing stage. Especially to all employees and workers of the Radio environment laboratory, Materials Physics Laboratory, and Betatron Laboratory.

R E F E R E N C E S

[1] *O. S. Chaudhary, M. Denaï, dan S. S. Refaat*, “Technology and Applications of Wide Bandgap Semiconductor Materials: Current State and Future Trends,” 2023.

[2] *S. Kanungo*, “2D materials-based nanoscale tunneling fi eld effect transistors : current developments and future prospects”, doi: 10.1038/s41699-022-00352-2.

[3] *S. Wang et al.,* “Review on the Application of Semiconductor Heterostructures in Photocatalytic Hydrogen Evolution: State-of-the-Art and Outlook,” 2023. Energy Fuels, vol. 37, no. 3, 1633–1656, doi: 10.1021/acs.energyfuels.2c03429.

[4] *H. H. Cheng, W. S. Yu, S. C. Tseng, Y. J. Wu, C. L. Hsieh, dan S. S. Lin*, “Reclaimed water in Taiwan : current status and future prospects,” 2023. doi: 10.1186/s42834-023-00177-8.

[5] *A. Kumar, A. Thorbole, dan R. K. Gupta*, “Sustaining the future: Semiconductor materials and their recovery,” 2025. Mater. Sci. Semicond. Process., vol. 185, 108943, doi: https://doi.org/10.1016/j.mssp.2024.108943.

[6] *T. Zhang et al*., "Overall design of CYCIAE-14, a 14 MeV PET cyclotron," Nucl. Instrum. Methods Phys. Res. Sect. B Beam Interact. Mater. At., 2011. vol. 269, no. 24, 2950–2954. doi: 10.1016/j.nimb.2011.04.049.

[7] *B. Li, B. F. Trueman, S. Munoz, J. A. Locsin, dan G. A. Gagnon,* "Impact of sodium silicate on lead release and colloid size distributions in drinking water," 2020. Water Res., 116709. doi: 10.1016/j.watres.2020.116709.

[8] *E. L. Foletto, E. Gratieri, L. H. De Oliveira, S. L. Jahn, dan S. M. Rs,* "Conversion of Rice Hull Ash into Soluble Sodium Silicate 2. Materials and Methods,". 2006. vol. 9, no. 3, 335–338.

[9] P. Chattopadhyay dan R. B. Gupta, "Supercritical CO2-Based Formation of Silica Nanoparticles Using Water-in-Oil Microemulsions," 2020. 465–472.

[10] *I. M. Joni, M. Vanitha, C. Panatarani, dan F. Faizal,* "Dispersion of amorphous silica nanoparticles via beads milling process and their particle size analysis, hydrophobicity and anti-bacterial activity," Adv. Powder Technol., 2019, doi: 10.1016/j.apt.2019.10.029.

[11] *Z. Liu et al*., "Tl-based wide gap semiconductor materials for x-ray and gamma ray detection," Chem. Biol. Radiol. Nucl. Explos. CBRNE Sens. XII, vol. 8018, 80180H, 2011, doi: 10.1117/12.883230.

[12] *L. Handayani, S. Aprilia, C. Rahmawati, T. B. Aulia, P. Ludvig, dan J. Ahmad*, "Sodium Silicate from Rice Husk Ash and Their Effects as Geopolymer Cement," 2022.

[13] *J. Qu, J. Zhang, H. Li, dan S. Li,* "Science of the Total Environment A high value utilization process for coal gasi fi cation slag : Preparation of high modulus sodium silicate by mechano-chemical synergistic activation," Sci. Total Environ., 2021. vol. 801, 149761, doi: 10.1016/j.scitotenv.2021.149761.

[14] *B. Ozpineci dan L. Tolbert*, "Comparison of wide-bandgap semiconductors for power electronics applications". 2004.

[15] *A. Chaves et al*., "Bandgap engineering of two-dimensional semiconductor materials," Npj 2D Mater. Appl., 2020. vol. 4, no. 1, doi: 10.1038/s41699-020-00162-4.

[16] *A. Goyal, P. Gorai, S. Anand, E. S. Toberer, G. J. Snyder, dan V. Stevanović*, "On the Dopability of Semiconductors and Governing Material Properties," Chem. Mater., 2020. vol. 32, no. 11, 4467–4480, doi: 10.1021/acs.chemmater.9b05126.

[17] *A. Charnas et al*., "Review—Extremely Thin Amorphous Indium Oxide Transistors," Adv. Mater., 2024. vol. 36, no. 9, doi: 10.1002/adma.202304044.

[18] *Wei B, Li L, Shao L, Wang J.* Crystalline-Amorphous Nanostructures: Microstructure, Property and Modelling. *Materials (Basel)*. 2023. vol. 16, no. 7. 2874. doi:10.3390/ma16072874

[19] *E. Görlich*, "The structure of SiO_2 - Current views," Ceram. Int., 1982. vol. 8, no. 1, 3–16, doi: 10.1016/0272-8842(82)90009-8.

[20] S. *A. Miller,* "The location of the chemical bond. Application of long covalent bond theory to the structure of silica," Front. Chem., 2023, vol. 11, no. February 1–18, doi: 10.3389/fchem.2023.1123322.

[21] *N. Nagasima*, "Structure analysis of thermal oxide films of silicon by electron diffraction and infrared absorption," Jpn. J. Appl. Phys., 1970. vol. 9, no. 8, 879–888, doi: 10.1143/JJAP.9.879.

[22] *L. Li et al*., "Theoretical studies on intrinsic electron traps in strained amorphous silica," J. Non-Cryst. Solids, 2023. vol. 613, 122396, doi: https://doi.org/10.1016/j.jnoncrysol.2023.122396.

[23] *M. A. Berding, A. Sher, dan A. B. Chen*, "Structural Properties of Bismuth-Bearing Semiconductor Alloys.," NASA Contract. Rep., 1986. vol. 63, no. January.

[24] *D. L. Ferreira et al*., "Size-dependent bandgap and particle size distribution of colloidal semiconductor nanocrystals," J. Chem. Phys., 2017. vol. 147, no. 15, doi: 10.1063/1.4999093.
[25] *L. Bläubaum, F. Röder, C. Nowak, H. S. Chan, A. Kwade, dan U. Krewer,* "Impact of Particle Size Distribution on Performance of Lithium-Ion Batteries," ChemElectroChem, 2020. vol. 7, no. 23, 4755–4766, , doi: 10.1002/celc.202001249.
[26] *J. Kreuter, E. Liehl, U. Berg, M. Soliva, dan P. P. Speiser,* "Influence of hydrophobicity on the adjuvant effect of particulate polymeric adjuvants," Vaccine, 1988. vol. 6, no. 3, 253–256, , doi: 10.1016/0264-410X(88)90220-4.
[27] *T. Dietl dan H. Ohno*, "Ferromagnetic III-V and II-VI semiconductors," MRS Bull., 2003. vol. 28, no. 10, 714–719, doi: 10.1557/mrs2003.211.
[28] *Z. Wang, P. K. Nayak, J. A. Caraveo-frescas, dan H. N. Alshareef,* "Recent Developments in p-Type Oxide Semiconductor Materials and Devices," 2016, 3831–3892, doi: 10.1002/adma.201503080.
[29] *B. H. Rho dan K. J. Lee*, "Development and validation of atmospheric dispersion: Computer program using tritium air concentrations in the environment around heavy water reactor power plants," Ann. Nucl. Energy, 1998, vol. 25, no. 14, 1119–1132, doi: 10.1016/S0306-4549(97)00103-5.
[30] I. Temiño *et al*., "Morphology and mobility as tools to control and unprecedentedly enhance X-ray sensitivity in organic thin-films," Nat. Commun., 2020. vol. 11, no. 1, 1–10, doi: 10.1038/s41467-020-15974-7.
[31] *X. Chen,* "Synthesis of high strength binders from alkali activation of glass materials from municipal solid waste incineration bottom ash," J. Clean. Prod., 2018. doi: 10.1016/j.jclepro.2018.11.295.
[32] *L. A. September, N. Kheswa, N. S. Seroka, dan L. Khotseng*, "Green synthesis of silica and silicon from agricultural residue sugarcane bagasse ash - a mini review," RSC Adv., 2023.vol. 13, no. 2, 1370–1380, doi: 10.1039/d2ra07490g.
[33] *C. Soc,* "Chem Soc Rev," Chem. Soc. Rev., 2018, vol. 47, 3152–3188, doi: 10.1039/c7cs00849j.
[34] *C. An et al*., "Long-Range Ordered Amorphous Atomic Chains as Building Blocks of a Superconducting Quasi-One-Dimensional Crystal," Adv. Mater., 2020. vol. 32, no. 38, 2002352 doi: 10.1002/adma.202002352.
[35] *D. A. Keen dan M. T. Dove, "*Local structures of amorphous and crystalline phases of silica, SiO_2 , by neutron total scattering," J. Phys. Condens. Matter, 1999. vol. 11, no. 47, 9263–9273, doi: 10.1088/0953-8984/11/47/311.
[36] *B. Wei, L. Li, L. Shao, dan J. Wang*, "Crystalline–Amorphous Nanostructures: Microstructure, Property and Modelling," Materials, 2023. vol. 16, no. 7, 2874, doi: 10.3390/ma16072874.
[37] *K. Bu et al*., "Nested order-disorder framework containing a crystalline matrix with self-filled amorphous-like innards," Nat. Commun., 2022. vol. 13, no. 1, 4650, doi: 10.1038/s41467-022-32419-5.
[38] *A. A. Bunaciu, E. G. Udriştioiu, dan H. Y. Aboul-Enein,* "X-Ray Diffraction: Instrumentation and Applications," Crit. Rev. Anal. Chem., 2015.vol. 45, no. 4, 289–299, doi: 10.1080/10408347.2014.949616.
[39] *S. Fatimah, R. Ragadhita, D. F. A. Husaeni, dan A. B. D. Nandiyanto,* "How to Calculate Crystallite Size from X-Ray Diffraction (XRD) using Scherrer Method," ASEAN J. Sci. Eng., 2021. vol. 2, no. 1, 65–76, doi: 10.17509/ajse.v2i1.37647.
[40] *H. Khan, A. S. Yerramilli, A. D'Oliveira, T. L. Alford, D. C. Boffito, dan G. S. Patience,* "Experimental methods in chemical engineering: X-ray diffraction spectroscopy— XRD," Can. J. Chem. Eng., 2020. vol. 98, no. 6, 1255–1266, doi: 10.1002/cjce.23747.

[41] *Ariyanti, D., et al*., One Stage Method: Activated Carbon Modified by Surfactant and Irradiation to Highly Improve Adsorption of Pb2+ Wastewater Simulation (Utilization of Banana Peel Biomass) J. Ecol. Eng. 2024. 25(12). 70-82.
[42] *Ariyanti, D., et al.*, Integration methods: H3PO4 immersion and gamma irradiation exposure in modified activated carbon from banana (Musa paradisiaca L. sp.) stems biomass. Journal of Physics: Conference Series. 2024. 2828. 1-6. doi:10.1088/1742-6596/2828/1/012024.
[43] A*riyanti, D., et al.,* Effect of Gamma ^{60}Co Irradiation on Morphology of Carbon/Lauryl Sulphate (Carbon/SLS) Using SEM-EDS. 2023. Malaysian Journal of Microscopy 19(2). 15-23.
[44] *Mănăilă-Maximean, D. and Cîrcu*, V. On liquid crystals and liquid crystal dispersions. 2022. Ann. Acad. Rom. Sci., Ser. Phys. Chem, 7(1). 88-98. DOI: 10.56082/annalsarsciphyschem.2022.1.88.
[45] *Soraya Nur I., et al.,* Extraction of Silica from Bengkulu Beach Sand using Alkali Fusion Method. 2020. PENDIPA Journal of Science Education 4 (2), 1-5.
[46] S*. I. Mudryi, et al.,* Evaluation of the Volume Fraction of the Crystalline Phase in Amorphous Alloys. 2005. Materials Science, 41 (3). 1-6.